Finite Strain Crack Tip Fields in Soft Incompressible Elastic Solids

Venkat R. Krishnan, Chung Yuen Hui,* and Rong Long

Department of Theoretical & Applied Mechanics, Cornell University, Ithaca, New York 14850

Received August 27, 2008. Revised Manuscript Received September 30, 2008

A finite element model (FEM) is used to study the behavior of the large deformation field near the tip of a crack in a soft incompressible plane stress fracture specimen loaded in mode I. Results are obtained for the case of a neo-Hookean solid (ideal rubber) and a hyperelastic solid with exponentially hardening behavior. In contrast to the predictions of linear elastic fracture mechanics (LEFM), the near tip stress fields are dominated by the opening stress which shows a $1/R$ singularity for the neo-Hookean material and a $-1/(R \ln R)$ singularity for the exponential hardening solid. We found very similar qualitative behavior in the near tip stress fields despite the very large difference in strain hardening behavior of the two material models. Our result shows that the near tip opening stress is controlled by the far field energy release rate for large applied loads.

1. Introduction

Fracture of soft materials such as gels has recently been of interest to physicists and chemists. The physical structure of these materials consists of a dense network of polymer chains in a liquid matrix giving rise to a high degree of elasticity, incompressibility, and strain hardening. However, their fracture behavior is not very well understood. Recent works on gel fracture has focused mainly on covalent hydrogels[1−4] or biopolymer gels such as gelatin.[5,6] As experimentalists have pointed out, gels made from polymerization of monomers in a cross-linking reaction are usually brittle with few dissipative mechanisms. On the other hand, double network (DN) gels have shown recently to possess high fracture toughness,[7] because of their ability to transmit stress concentrations at crack tips between the cross-linking networks. However, DN gels are not very elastic and show hysteresis on repeated loading due to structural changes during loading.[8] Recently, there have been several efforts to perform carefully designed fracture experiments on well-characterized, elastic polymer gels. For example, using a fracture specimen with a strip geometry (see Figure 1), Baumberger et al.[9] studied the fracture behavior of gelatin gels. They found that gelatin is very elastic at small strains. No systematic large strain measurement was done, and fracture images suggest that gelatin is highly dissipative above a certain level of strain. A similar fracture study using the same specimen made with an acrylic triblock copolymer gel was carried out by Seitz et al.[10]

The nature of cracks in soft elastic materials is qualitatively very different from those in metals and other commonly known brittle materials such as polymer glass and ceramics, in that soft materials exhibit very large deformation and a high degree of strain hardening as deliberated by Shull.[11] However, theoretical models of the stress and deformation fields near the tips of cracks in soft materials are mostly based on the assumption of small deformations and linear elastic behavior. Although there have been some beautiful analyses on the nonlinear deformation fields

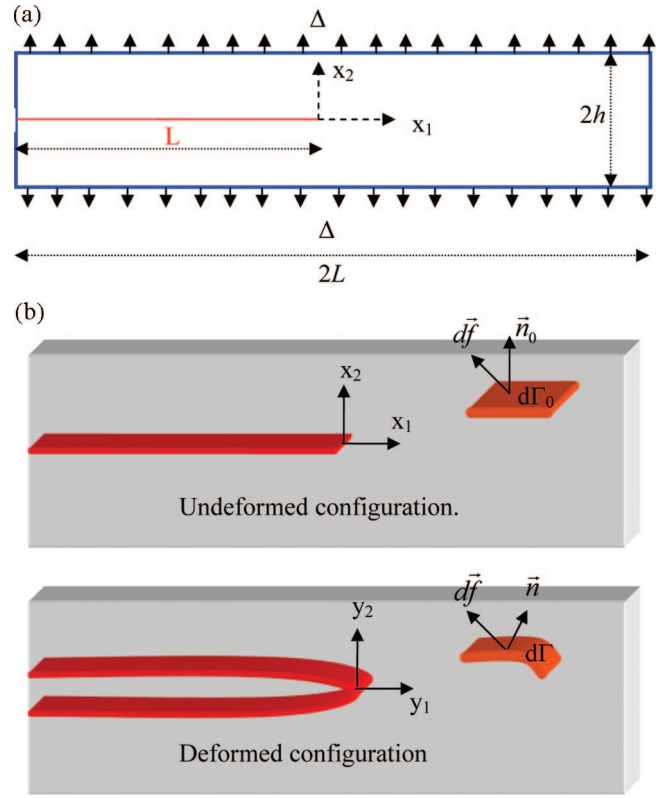

Figure 1. (a) Side view schematic of strip specimen. The out-of-plane thickness is very small in comparison with h, which is much less than L. Δ is the applied displacement. (b) Undeformed and deformed geometries of strip specimen showing first Piola Kirchoff stress ($\boldsymbol{S}$) and true stress ($\boldsymbol{T}$). Briefly, let $\mathrm{d}\vec{f}$ be the force acting on a material surface of area $\mathrm{d}\Gamma_o$ in the undeformed configuration with the unit normal vector $\vec{n}_o$; after deformation, $\mathrm{d}\Gamma_o$ becomes $\mathrm{d}\Gamma$ with new unit normal vector $\vec{n}$. The first Piola Kirchoff stress tensor $\boldsymbol{S}$ is defined by $\mathrm{d}\vec{f} = \boldsymbol{S}\vec{n}_o\,\mathrm{d}\Gamma_o$. The true (Cauchy) stress tensor $\boldsymbol{T}$ is defined by $\mathrm{d}\vec{f} = \boldsymbol{T}\vec{n}\,\mathrm{d}\Gamma$. Here bold letter denotes a second-order tensor.

* Corresponding author. E-mail: ch45@cornell.edu.

(1) Tanaka, Y.; Fukao, K.; Miyamoto, Y. *Eur. Phys. J. E* **2000**, *3*(4), 395–401.
(2) Tanaka, Y.; Fukao, K.; Miyamoto, Y.; Nakazawa, H.; Sekimoto, K. *J. Phys. Soc. Jpn.* **1996**, *65*(8), 2349–2352.
(3) Livne, A.; Ben-David, O.; Fineberg, J. *Phys. Rev. Lett.* **2007**, *98*(12), 124301.
(4) Livne, A.; Cohen, G.; Fineberg, J. *Phys. Rev. Lett.* **2005**, *94*(22), 224301.
(5) Barrangou, L. M.; Daubert, C. R.; Foegeding, E. A. *Food Hydrocolloids* **2006**, *20*(2−3), 184–203.
(6) Baumberger, T.; Caroli, C.; Martina, D. *Eur. Phys. J. E* **2006**, *21*(1), 81–89.
(7) Gong, J. P.; Katsuyama, Y.; Kurokawa, T.; Osada, Y. *Adv. Mater.* **2003**, *15*(14), 1155.
(8) Webber, R. E.; Creton, C.; Brown, H. R.; Gong, J. P. *Macromolecules* **2007**, *40*(8), 2919–2927.
(9) Baumberger, T.; Caroli, C.; Martina, D. *Nat. Mater.* **2006**, *5*(7), 552–555.
(10) Seitz, M. E.; Shull, K. R.; Krishnan, V. R.; Hui, C. Y.; Martina D.; Baumberger, T. *Soft Matter*, http://dx.doi.org/10.1039/b810041a.
(11) Shull, K. R. *J. Polym. Sci., Part B: Polym. Phys.* **2006**, *44*, 3436–3439.

10.1021/la802795e CCC: $40.75
Published on Web 11/20/2008

near cracks in hyperelastic solids,[12−16] these analyses are very mathematical and are not easily accessible to material scientists and chemists. There are also very few numerical studies of crack tip fields in real fracture specimens. An example of such a study is that by Ravichandran and Knauss.[17] They used a Lagrangian-based finite element model (FEM) to study the finite strain field of an interface crack between two infinite hyperelastic sheets.

In this paper, we address the nonlinear deformation of the crack tip fields in soft elastic solids in a way that is accessible to experimentalists who are interested in the fracture of soft materials. In section 2, we focus attention on a neo-Hookean solid. We determine the stress fields near the crack tip and relate these stresses to the external applied load of a fracture specimen. Our results on the near tip fields are based on the analysis of Guebelle and Knauss;[16] we also included many features of their solutions which have not been discussed previously and which are of practical relevance. The full-field solution for the neo-Hookean solid is new and is obtained using a nonlinear finite element analysis. In section 3, we study the crack tip field in the strip specimen using a constitutive model that has very severe strain hardening. A summary and discussion are given in section 4.

One may question our choice of studying a neo-Hookean solid since real gels or rubber exhibits finite extensibility and strain hardening much more than this idealized model. There are several reasons to study the neo-Hookean solid. First, it is one of the few elastic materials which have universal appeal and where an exact closed form solution of the crack tip fields is known. Furthermore, even for this simple material, the solution is not readily accessible in the literature. For example, the results presented in the literature do not determine the true stress fields near the crack tip in the deformed coordinates. Second, this solution allows us to validate the accuracy of our numerical method. In section 2, the same numerical technique is used to study the stress fields in a real hydrogel specimen. Finally, by comparing the neo-Hookean solution with the numerical solution of a severe strain hardening material, we discover that many aspects of the neo-Hookean solution are universal and therefore allow us to gain insight into the fracture mechanics of soft materials.

2. Fracture Mechanics of a Neo-Hookean Solid under Plane Stress

2.1. Strip Specimen. To put our problem into perspective, we focus on the fracture specimen used by Baumberger et al.[9] and Seitz et al.[10] to study the fracture of gels. The specimen consists of a long elastic strip of width $2L$ with height $2h$, $L \gg h$. The out-of-plane thickness of the strip t is assumed to be much smaller than h so that the strip is loaded in plane stress. A schematic of the undeformed reference configuration of the specimen is shown in Figure 1. An in-plane Cartesian coordinate system (x_1,x_2) is placed at the undeformed crack tip. Before deformation, the crack is a slit of length L and is located at the midplane $x_2 = 0$. The sample is stretched by applying a spatially uniform vertical displacement $u_2 = \pm\Delta$ at the top and bottom faces ($x_2 = \pm h$) resulting in a uniform stretch ratio of $\lambda_a = 1 + \Delta/h$ at distances far ahead of the crack tip.

2.2. Crack Tip Fields for a Neo-Hookean Solid. Let y_α ($\alpha = 1, 2$) denote the deformed coordinates of a material point located at x_α. Also, let ($r \equiv \sqrt{(x_\alpha x_\alpha)}$,$\theta$) be a polar coordinate system describing the position of a material point x_α in the reference undeformed configuration. We place the origin of the deformed coordinates y_α at the deformed crack tip; that is, $y_\alpha(r = 0) = 0$. We will use the Einstein summation convention (sum over repeated indices) throughout this work. The displacements $u_\alpha(x_1,x_2)$ of a material point at x_α are related to y_α by

$$y_\alpha = x_\alpha + u_\alpha \tag{1}$$

In the following, we consider mode I deformation, where y_1 and y_2 are even and odd functions of x_2, respectively. This condition is satisfied by the loading of our strip specimen. In plane stress, the strain energy density of a neo-Hookean solid W was first given by Rivlin[18]

$$W = \frac{\mu}{2} I_1 \tag{2}$$

where

$$I_1 \equiv y_{\alpha,\beta} y_{\alpha,\beta} + \lambda^2 - 3 \tag{3}$$

In (3), λ is the stretch ratio in the out-of-plane direction.

2.3. Near Tip Displacement Fields. Near the crack tip, Guebelle and Knauss[16] have shown that

$$y_\alpha(r \to 0, \theta) = \begin{cases} y_1 = C_1 r \cos\theta + o(r) \\ y_2 = C_2 r^{1/2} \sin(\theta/2) + o(r^{1/2}) \end{cases} \qquad -\pi \le \theta \le \pi \tag{4}$$

Equation 4 can also be derived from a first-order approximate full field solution in an earlier work by Wong and Shield.[12] C_α values in (4) are unknown constants which depend on the external loads (in our case λ_a) and the specimen geometry. It is for this reason that these constants cannot be determined by asymptotic analysis. Note that C_2 has a unit of square root of length while C_1 is dimensionless. In fact, C_1 in (4) can be interpreted as the horizontal stretch ratio of a material element close to the crack tip. Equation 4 implies that the deformed crack profile is

$$y_2 = \pm C_2 \sqrt{\frac{-y_1}{C_1}}, \qquad y_1 \to 0^- \tag{5}$$

2.4. Near Tip Stresses. The first Piola Kirchoff stress $S_{\alpha\beta}$ (Figure 1b) in the reference configuration can be determined using (2) and (4). It is[16]

$$S_{11} = \mu C_1, \quad S_{12} = 0, \quad S_{21} = -\frac{\mu C_2}{2} r^{-1/2} \sin(\theta/2),$$
$$S_{22} = \frac{\mu C_2}{2} r^{-1/2} \cos(\theta/2); \qquad r \to 0, \ -\pi \le \theta \le \pi \tag{6}$$

The physically relevant stress measure is the true (Cauchy) stress $T_{\alpha\beta}$ in the deformed configuration. The true stress components are related to the first Piola Kirchoff stress by $T_{\alpha\beta} = S_{\alpha\xi} y_{\beta,\xi}$, where $y_{\beta,\xi}$ denotes $\partial y_\beta/\partial x_\xi$. Using (4) and (6), the true stresses as $r \to 0$ are

$$T_{11} = \mu C_1^2, \quad T_{22} = \mu C_2^2/4r \tag{7a}$$

$$T_{12} = T_{21} = -\frac{\mu C_2 C_1}{\sqrt{2r}} \sin(\theta/2) \tag{7b}$$

For a *linear* elastic solid, the crack tip stresses in mode I is[19]

(12) Wong, F. S.; Shield, R. T. *Z. Angew. Math. Phys.* **1969**, *20*(2), 176–199.
(13) Knowles, J. K.; Sternberg, E. *J. Elasticity* **1973**, *3*(2), 67–107.
(14) Knowles, J. K.; Sternberg, E. *J. Elasticity* **1974**, *4*(3), 201–233.
(15) Stephenson, R. A. *J. Elasticity* **1982**, *12*(1), 65–99.
(16) Geubelle, P. H.; Knauss, W. G. *J. Elasticity* **1994**, *35*(1−3), 61–98.
(17) Ravichandran, G.; Knauss, W. G. *Int. J. Fract.* **1989**, *39*, 235–253.
(18) Rivlin, R. *R. Soc. London: Philos. Trans., Ser. A* **1948**, *240*, 509–525.
(19) Rice, J. R. *J. Appl. Mech.* **1968**, *35*(2), 379–386.

$$\begin{pmatrix} T_{11} \\ T_{22} \\ T_{12} \end{pmatrix} = \frac{K_I}{\sqrt{2\pi r}} \cos\frac{\theta}{2} \begin{pmatrix} 1 - \sin\frac{\theta}{2}\sin\frac{3\theta}{2} \\ 1 + \sin\frac{\theta}{2}\sin\frac{3\theta}{2} \\ \sin\frac{\theta}{2}\cos\frac{3\theta}{2} \end{pmatrix}; \qquad r \to 0 \quad (8)$$

where K_I is the mode I stress intensity factor. For our strip geometry K_I is found to be $2\sqrt{3\mu\Delta}/\sqrt{h}$ (see (18) in section 2.5). In linear elastic fracture mechanics (LEFM), the deformation field for a mode I crack depends on only one constant, K_I. Furthermore, *all* stress components have the *same* inverse square root singularity with distance from the crack tip, with the singularity being independent of direction. However, the nonlinear theory predicts that $T_{22} \propto 1/r$, T_{11} bounded, and $T_{12} \propto 1/\sqrt{r}$. In particular, directly ahead of the crack tip, LEFM predicts $T_{11} = T_{22}$, whereas $T_{11}/T_{22} \approx 0$ in the nonlinear theory. The amplitudes of the true stress near tip fields in the nonlinear theory are governed by *two* independent parameters, C_1 and C_2, whereas in the linear theory the amplitude is completely determined by a single parameter, K_I. A comparison of (7a), (7b), and (8) shows that the angular distributions of the stresses are very different. For example, the normal stress T_{22} in the nonlinear theory is independent of orientation in the reference coordinates. Note that the shear stress in the linear theory for positive angles less than 60° is *positive*, whereas this stress is *negative* for all positive angles in the nonlinear theory. The fact that the shear stress has a lower singularity than the normal stress implies that material points near the crack tip are under a state of *uniaxial* tension. Finally, note that the LEFM predicts that the stress state directly ahead of the crack tip ($\theta = 0$) is that of hydrostatic tension.

The true stresses in (7a) and (7b) are expressed in terms of the reference coordinates (Figure 1b). In practice, it is useful to express them in terms of the deformed coordinates y_α. A straightforward calculation using (4) shows that near the crack tip

$$r = \frac{2}{{C_2}^2}{y_2}^2 + \frac{y_1}{C_1}, \qquad \cos\theta = \frac{{C_2}^2 y_1}{2C_1{y_2}^2 + {C_2}^2 y_1} \quad (9)$$

Let (R,ϕ) denote a polar coordinate system located at the deformed crack tip, that is

$$y_1 = R\cos\phi, \qquad y_2 = R\sin\phi \quad (10a)$$

Equation 5 implies that near the crack tip

$$0 \le |\phi| < \frac{\pi}{2} \quad (10b)$$

Using (7a), (7b), and (9), the near tip true stresses (Figure 1b), valid in the sector $0 \le |\phi| < \pi/2$, are

$$T_{11} = \mu{C_1}^2 \quad (11a)$$

$$T_{22} = \frac{\mu{C_1}^2}{4\rho} f_{22}(\rho,\phi), \qquad f_{22}(\rho,\phi) = \frac{1}{2\rho\sin^2\phi + \cos\phi} \quad (11b)$$

$$T_{12} = T_{21} = \frac{\mu{C_1}^2}{\sqrt{\rho}} f_{12}(\rho,\phi),$$

$$f_{12}(\rho,\phi) = \frac{-\mathrm{sign}(\phi)(2^{-3/2})}{\sqrt{2\rho\sin^2\phi + \cos\phi}}\left(1 - \frac{\cos\phi}{2\rho\sin^2\phi + \cos\phi}\right)^{1/2} \quad (11c)$$

where ρ is a dimensionless distance from the deformed crack tip defined by

$$\rho \equiv RC_1/{C_2}^2 \quad (11d)$$

and

$$\mathrm{sign}(\phi) = 1(-1); \qquad \phi > 0\ (\phi < 0) \quad (11e)$$

Equations 11b and 11c imply that, as long as $|\phi| < \pi/2$, T_{22} and T_{12} can be approximated by taking $\rho \to 0$ in f_{22} and f_{12}. This results in

$$f_{22} \approx \sec\phi; \qquad \frac{\pi}{2} - |\phi| \ll 2\rho \quad (12a)$$

$$f_{12}(\phi) \approx \frac{-\sqrt{\rho}\tan\phi}{2}; \qquad \frac{\pi}{2} - |\phi| \ll 2\rho \quad (12b)$$

Using (10b), (11c), and (12b), the near tip shear stress is given by

$$T_{12} = T_{21} = -\frac{\mu{C_1}^2}{2}\tan\phi; \qquad \frac{\pi}{2} - |\phi| \ll 2\rho \quad (13)$$

in the deformed coordinates. Equation 13 states that the asymptotic shear stress is *bounded* and *independent of radius* in the sector $|\phi| - \pi/2 \ll \rho$! On the other hand, for $\rho > 0$, $|\phi| \to \pi/2$, we have

$$T_{22}(\rho, \phi \to \pi/2) = \mu\frac{{C_1}^2}{2\rho^2}; \qquad |\phi| \to \pi/2 \quad (14a)$$

$$T_{12} = T_{21} = -\mathrm{sign}(\phi)\frac{\mu{C_1}^2}{4\rho}; \qquad |\phi| \to \pi/2 \quad (14b)$$

That is, the normal and shear stresses are extremely concentrated on the deformed crack faces. The singularity of the normal stress T_{22} directly ahead of the crack tip is lower than that along the crack face. Also, the near tip shear stress is bounded away from the crack face; hence the near tip stress field is approximately uniaxial.

2.5. Energy Release Rate and the Determination of C_2. One of the constants C_2 can be determined using an energy argument. The energy release rate J for the strip geometry was first obtained by Sawyers and Rivlin.[20] For the case of a neo-Hookean solid, it is

$$J = h\mu\left(\lambda_a - \frac{1}{\lambda_a}\right)^2 \quad (15)$$

J can also be obtained using the path independent integral of Eshelby:[21]

$$J = \int_\Gamma (Wn_1 - S_{\alpha\beta}n_\beta u_{\alpha,1})\,\mathrm{d}s \quad (16)$$

where Γ is any simple closed path which encloses the crack tip in the reference configuration, n_β is the outward unit vector normal to Γ, and s denotes arc length. The path independence of the J integral allows us to choose Γ as a circular contour with arbitrarily small radius ε. The center of the circle coincides with the crack tip in the reference configuration. Since ε is arbitrarily small, the asymptotic fields given by (4) and (6) are exact on the circular path. Using (4) and (6), the J integral is found to be

$$J = \frac{\pi}{4}\mu{C_2}^2 \quad (17)$$

C_2 is found by equating (15) and (17), i.e.

(20) Sawyers, K. N.; Rivlin, R. S. *Eng. Fract. Mech.* **1974**, *6*(3), 557–562.
(21) Eshelby, J. D. *Proc. R. Soc. London, Ser. A: Math. Phys. Sci.* **1957**, *241*(1226):), 376–396.

$$C_2 = 2\sqrt{\frac{h}{\pi}}\left(\lambda_a - \frac{1}{\lambda_a}\right) \tag{18}$$

Note, for the special case of small applied strains, $\Delta/h \ll 1$

$$C_2 \approx 4\sqrt{\frac{1}{\pi h}}\Delta, \qquad J \approx 4\mu\Delta^2/h \tag{19}$$

According to LEFM,[19] $J \approx K_I^2/3\mu$. Using (19)

$$K_I = \frac{2\sqrt{3}\mu\Delta}{\sqrt{h}} \tag{20}$$

The determination of C_1 requires a full field analysis and will be presented in section 2.8.

2.6. Region of Validity of Near Tip Fields. The stress fields given by (11a) are valid in a small region Ω surrounding the crack tip. Let the linear dimension of Ω be denoted by d. To estimate d, consider the scenario of "small scale yielding" (SSY). SSY is satisfied when the applied stretch on the strip is small, that is, $\lambda_a \approx 1$ or $\Delta/h \ll 1$. Under SSY, the nonlinearity due to geometry changes and material behavior is confined to a very small region near the crack tip, that is, $d \ll h$. As a consequence, the LEFM solution (8) is valid at distances from the crack tip that are small compared with h but large compared with d. Using (8), the opening stress directly ahead of the crack tip is

$$T_{22} \approx \frac{K_I}{\sqrt{2\pi R}}, \qquad \text{where } d \ll R \ll h \tag{21}$$

We estimate d by equating (21) to (11b) at $R = d$ with $\phi = 0$ and using K_I given by (20). This gives

$$d \sim \frac{8C_1^2}{3\pi}\varepsilon_a^2 h \tag{22}$$

where $\varepsilon_a \equiv \Delta/h \ll 1$ is the applied strain. Equation 22 indicates that the region of dominance of the large strain asymptotic solution given by (11b) is proportional to the square of the applied strain. For example, for $\varepsilon = 0.1$ (marginally small strains), $d \sim (8.49 \times 10^{-3})h$ assuming that $C_1 = O(1)$. Since the region of dominance of the near tip fields must be less than d, very fine meshes are needed to resolve the near tip stresses in this limit.

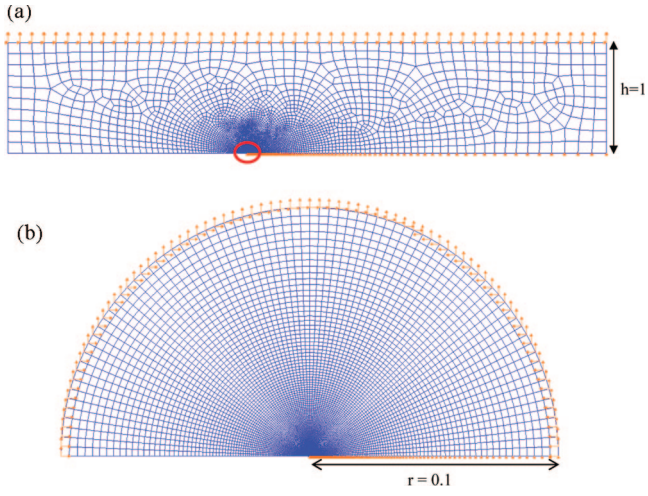

Figure 2. (a) FE model (coarse mesh) of half the specimen. A uniform vertical displacement is applied on the top edge. The horizontal displacement on the top edge is constrained to be zero. The submodel region ($r = 0.1$) is highlighted. (b) Semicircular FE submodel with fine mesh.

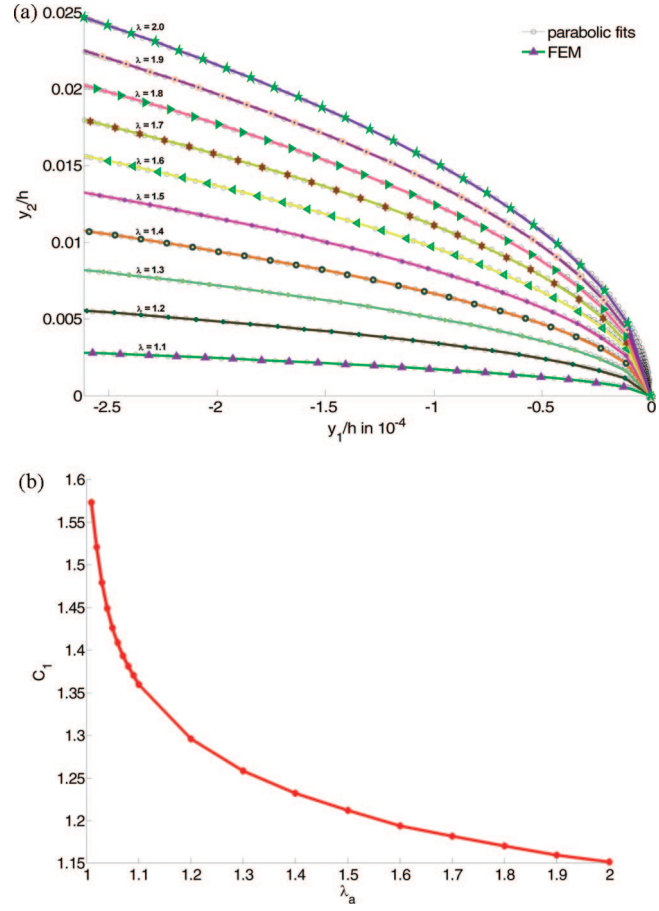

Figure 3. (a) Deformed crack profiles and their parabolic fits. (b) Dependence of C_1 on λ_a.

2.7. Finite Element Method (FEM). We solve the strip problem numerically using ABAQUS, a nonlinear finite element software. Our goals are to determine C_1 and to obtain the full-field solution. In addition, checking against the asymptotic solution for the neo-Hookean case is a stringent test of our FEM.

ABAQUS uses a total Lagrangian solution procedure for finite deformation hyperelastic material models. We implemented a python script to create the strip geometry and mesh for the FEM study (Figure 2a). Our two-dimensional FE model consists of quadrilateral elements (CPS4) with two degrees of freedom at each node. While ABAQUS has a material model for the neo-Hookean solid, the exponentially hardening solid required a user material (U-HYPER) subroutine to be written in Fortran, which is called by the ABAQUS solver during the solution procedure. Symmetry allows us to model only half the strip. We normalize all dimensions by h, half the initial height of the strip.

Determining the stress fields near the crack tip is nontrivial. For small applied strains, the region of validity of the $1/R$ singularity is very small and requires a very fine mesh near the crack tip to resolve the fields there accurately. In order to determine the near tip stresses, we follow a procedure known as submodeling.[22] The element size (e) in our FE mesh near the crack tip has to be on the order of $e \approx 10^{-6}$ in order to resolve the stresses. However, $e \approx 10^{-1}$ far from the crack tip. Hence, using $e \approx 10^{-6}$ close to the crack tip gives rise to a large condition number for the FE solution matrix, resulting in large relative errors. This can be avoided using a fine mesh everywhere, but will result in millions of degrees of freedom, making it intractable to solve on a single processor desktop.

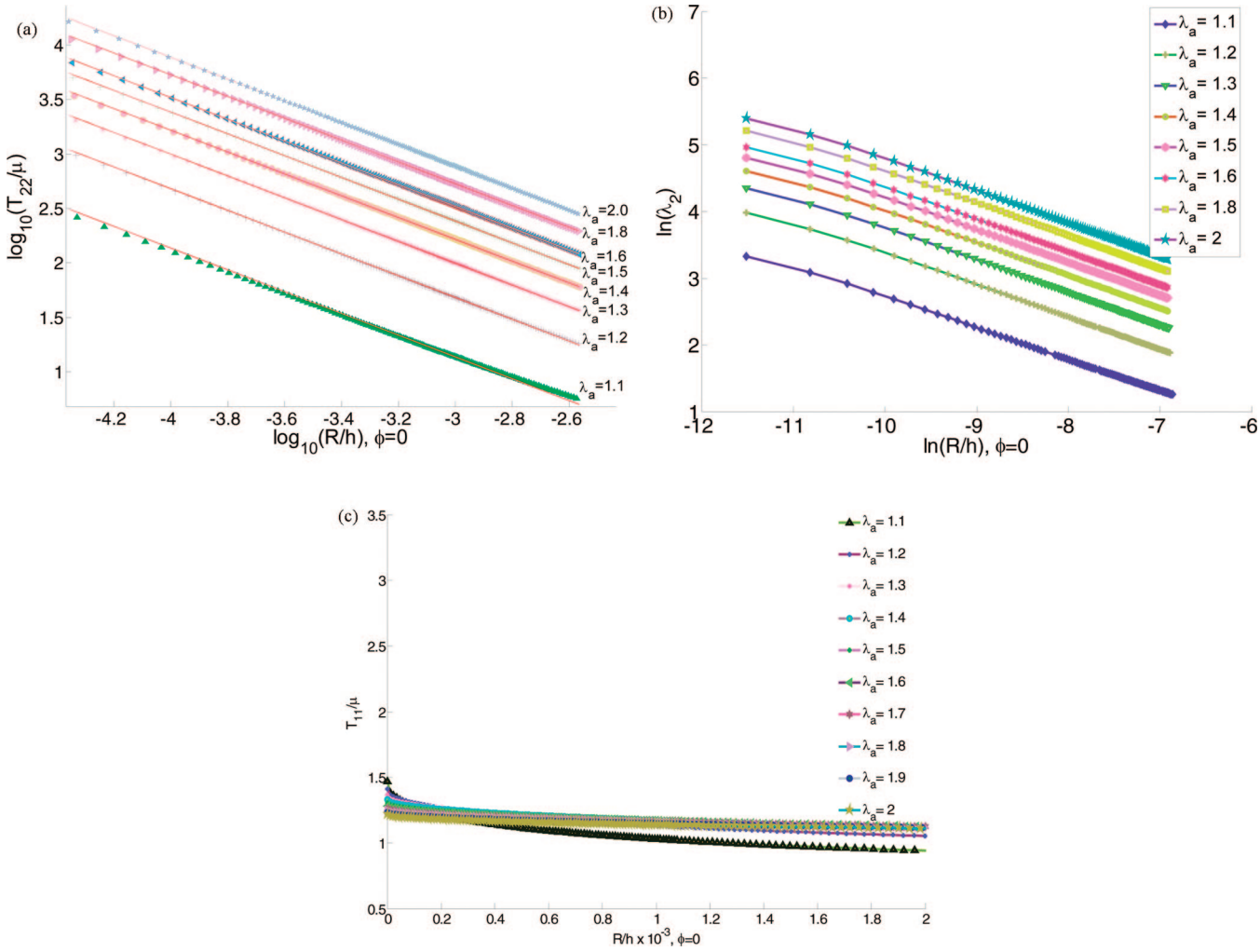

Figure 4. (a) log−log plot of T_{22} versus y_1/h showing a $1/R$ singularity as predicted by theory (24) [$1.1 \le \lambda_a \le 2.0$]. Symbols show FEM results, and solid lines show the fits with slope −1. (b) ln−ln plot of principal normal opening stretch λ_2 directly ahead of the crack tip. (c) T_{11} directly ahead of the crack tip in deformed coordinates.

To implement submodeling, we first run an analysis with a coarse mesh on the full model geometry and then reuse the results from the coarse mesh model as boundary conditions for a submodel with a finer mesh (Figure 2b). The submodel is a semicircle of radius $r = 10^{-1}$ centered at the crack tip. A convergence study was carried out to ensure that the coarse mesh results are accurate at the boundary of the submodel. We also verified that the coarse mesh results agree with the submodel results at the boundary. A simple way to check the accuracy of our simulations is to note that, at distances sufficiently far from the crack tip, the normal Cauchy stress is approximately independent of x and is given by[10]

$$T_{22} = \mu\left(\lambda_a^{\,2} - \frac{1}{\lambda_a^{\,2}}\right) \tag{23}$$

Our simulations show that (23) is satisfied within 0.01% at distances $R > 2h$.

2.8. Numerical Results for Neo-Hookean Solid. Recall from (5) that $y_2 = \pm C_2\sqrt{(-y_1/C_1)}$, where C_2 is given by (18). This result allows us to determine C_1 from FEM analysis by fitting parabolas to the deformed crack profiles close to the crack tip at successive levels of λ_a. The crack profiles and their parabolic fits are shown in Figure 3a, and the plot of C_1 vs λ_a is shown in Figure 3b.

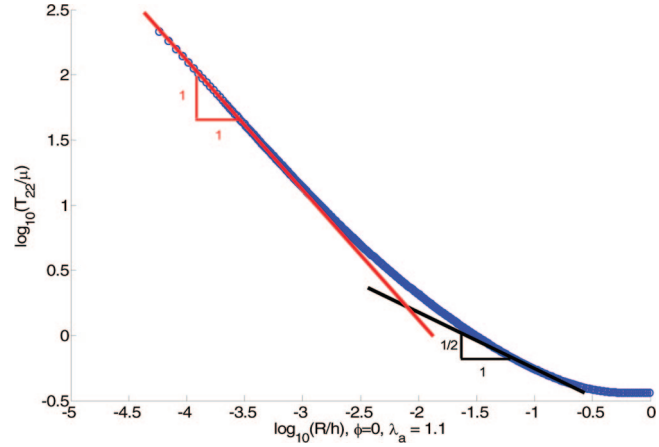

Figure 5. Normal stress T_{22} vs distance from crack tip, R ($\phi = 0$) under SSY ($\lambda_a = 1.1$). Close to the crack tip, it exhibits a $1/R$ singularity, and away from it, the $1/\sqrt{R}$ singularity takes over.

$C_1(\lambda_a)$ can also be determined by fitting the normal true stresses T_{22} ahead of the crack tip for different levels of applied deformation. The true stress T_{22}/μ predicted by the asymptotic

(22) Hibbit Karlsson and Sorensen Inc. *ABAQUS Manuals*, Abaqus 6.6; Hibbit Karlsson and Sorensen Inc.: Providence, RI, 2007.

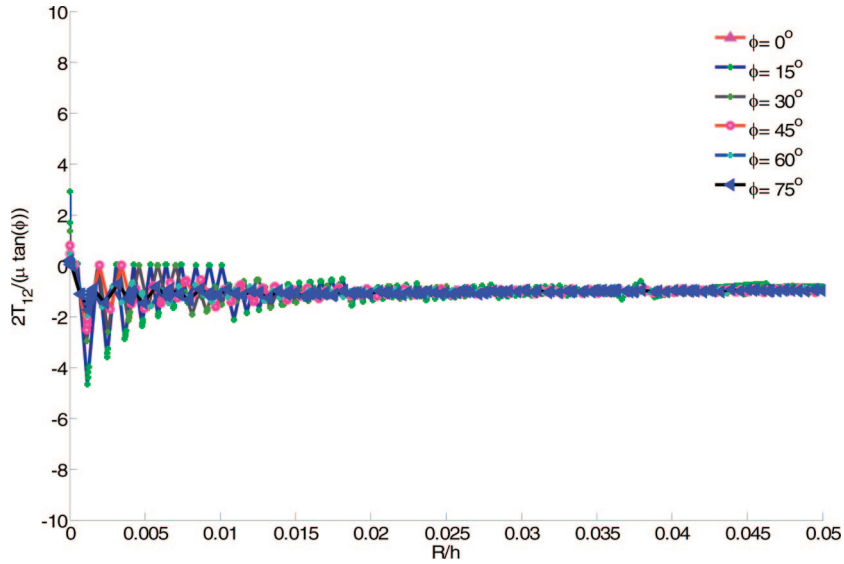

Figure 6. $^{-}\bar{T}_{12} \equiv 2T_{12}/\mu \tan \phi$ plotted along different angles ahead of crack tip for $\lambda_a = 2.0$. As predicted by (13), $\bar{T}_{12}$ is independent of R and ϕ.

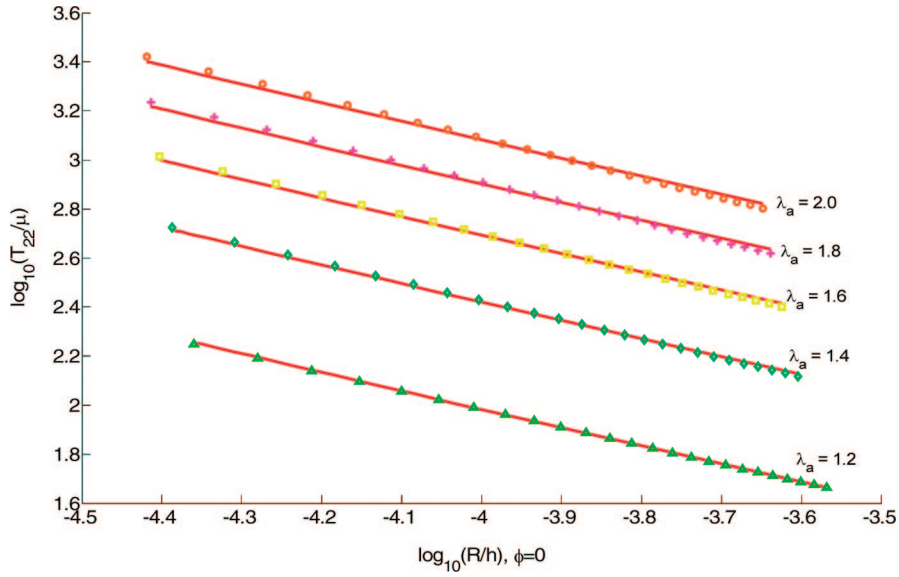

Figure 7. log−log plot of T_{22}/μ versus y_1/h for $I_m = 3.5$ for different applied stretch λ_a values. The fits (solid lines) are based on (26a). The finite element results are shown as symbols.

theory can be obtained by combining (10b), (11b), and (17), which gives

$$T_{22}(R \to 0, \phi = 0) = \frac{C_1 J}{\pi R} \tag{24}$$

where $J = \mu h(\lambda_a - 1/\lambda_a)^2$, recalling (15). If the FE result is accurate near the crack tip, $C_1(\lambda_a)$ values computed from fitting the crack profiles and the normal true stresses have to be the same. This is indeed the case as shown in Figure 4a, where $C_1(\lambda_a)$ obtained from Figure 3b is used to fit the normal true stress T_{22} ahead of the crack tip. Numerical results for the normal opening stretch λ_2 are plotted in a ln−ln plot in Figure 4b. The local stretch near the crack tip is almost 150 times the applied far field stretch. The transverse normal opening stress (T_{11}/μ) directly ahead of the crack tip is plotted in Figure 4c and shows no dependence on distance from crack tip (R) as predicted by asymptotic theory.

Figure 4b,c shows that T_{11} ahead of the crack tip is about 3 orders of magnitude smaller than T_{22}, and consistent with (10a), it approaches a constant value as dictated by the asymptotic analyses. Since the applied strip displacement λ_a is close to 1, SSY condition is valid. From section 2.6 (for small applied stretch $\lambda_a \approx 1$), LEFM should apply so that $T_{22} \propto 1/\sqrt{R}$ in the region $d \ll R \ll h$. In this region, a log−log plot of the true stress T_{22} versus R is a straight line with a slope of −1/2. On the other hand, for $R \ll d$, (23) suggests that a log−log plot of the true stress versus R is a straight line with slope −1. This hypothesis is in good agreement with the result as shown in Figure 5.

Finally, the near tip shear stress field $\bar{T}_{12} \equiv 2T_{12}/\mu \tan \phi$ vs R/h is shown in Figure 6 for $\lambda_a = 2.0$ and for different angles ϕ. Consistent with (13), the shear stress normalized by $\mu \tan \phi$ is independent of ϕ and approaches a constant for $|\phi| < \pi/2$.

3. Crack Tip Fields in a Strain Hardening Material

The neo-Hookean model underestimates the strain hardening of elastomers. This inadequacy motivates us to study the crack

(23) Krishnan, V. R.; Hui, C. Y. *Soft Matter* **2008**, *4*, 1909–1915.

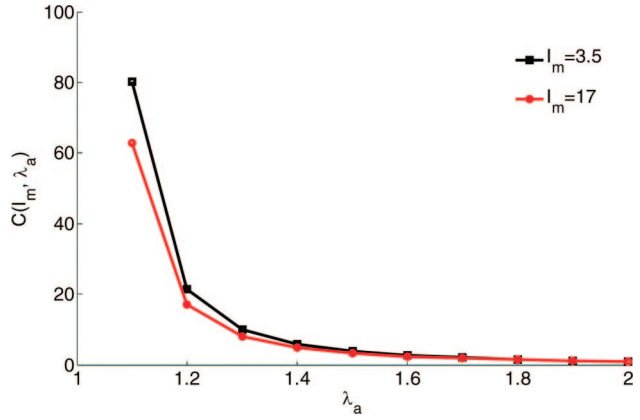

Figure 8. $C(I_m,\lambda_a)$ vs λ_a.

tip field of a material that exhibits very severe strain hardening. The constitutive model used in this study is motivated by the recent fracture experiments of Seitz et al.[10] Their fracture specimen is the strip geometry which is shown schematically in Figure 1. The specimen is an elastic hydrogel which consists of acrylic triblock copolymers with poly(methyl methacrylate) [PMMA] endblocks and a poly(*n*-butyl acrylate) [PnBA] midblock. They found a strain energy density function W[10,23] that fits their uniaxial compression data well. In plane stress, the strain energy density is given by

$$W = \frac{\mu}{2} I_m \left(\exp\left(\frac{I_1}{I_m} \right) - 1 \right) \tag{25a}$$

where μ is the small strain shear modulus, I_1 is defined in (3), and I_m is a strain hardening parameter. Note that, for small strains, this material behaves like a neo-Hookean solid, i.e.

$$W(I_1 \ll 1) \approx \frac{\mu}{2} I_1 \tag{25b}$$

For large strains (i.e., $I_1/I_m \gg 1$), the material hardens exponentially. This feature allows us use this model to study the nature of crack tip fields in materials with finite extensibility. Depending on the length of the midblocks and the weight percent of polymer used, the small strain shear modulus in their experiments varies from 2.7 to 6.4 kPa. Upon fitting, the strain hardening parameter I_m is found to vary from 3.5 to 17. The asymptotic behavior of the near tip fields in a material governed by this work function is not known. In fact, asymptotic analysis becomes much more difficult as strain hardening increases. For example, Guebelle and Knauss[16] considered a generalized neo-Hookean model with energy density function

$$W = \frac{\mu}{2b}\left[\left(1 + \frac{b}{n} I_1 \right)^n - 1 \right] \tag{26a}$$

where b is a material constant and $n > 1/2$ is a strain hardening parameter. In this model, strain hardening increases with n. They discovered that their asymptotic analysis breaks down for $n > 7/5$. It is interesting to note that

$$\lim_{n\to\infty} \frac{\mu}{2b}\left[\left(1 + \frac{b}{n} I_1 \right)^n - 1 \right] = \frac{\mu}{2b}[\exp(bI_1) - 1] \tag{26b}$$

In this limit, the generalized neo-Hookean model is the same as the exponential model for $b = 1/I_m$. In this section, we determine these near tip fields using our nonlinear finite element model.

3.1. Results for an Elastomer Which Strains Hardens Exponentially. The experiments of Seitz et al.[10] were conducted in the range of moderately large applied stretches, i.e., $\lambda_a \approx 2$; therefore, simulations have been carried out for moderate and large deformations. A log−log plot of the true stress directly ahead of the crack tip ($\phi = 0$) is plotted in Figure 7 for several applied stretches λ_a and for $I_m = 3.5$. We discovered that

$$T_{22}/\mu \propto -1/(R \ln R) \tag{27}$$

fits the FE results very well. Our numerical results suggest that

$$T_{22}(R \to 0, \phi = 0) = -C(I_m, \lambda_a) J/(R \ln R) \tag{28}$$

where $C(I_m,\lambda_a)$ is a dimensionless function of λ_a; J is the energy release rate and is found to be

$$J = \mu h I_m \left(\exp\left(\frac{I_1}{I_m} \right) - 1 \right), \qquad I_1 = \lambda_a^2 + \frac{1}{\lambda_a^2} - 2 \tag{29}$$

for the strip specimen.[10] Note that C in (28) plays the same role as C_1 for the neo-Hookean solid. The nature of the normal opening true stress (T_{22}) as given by (27) was independent of the value chosen for I_m, and we obtained similar results for $I_m = 17$.

As in the neo-Hookean case, we determine $C(I_m,\lambda_a)$ by plotting log T_{22} versus log R and finding the intercepts of the resulting

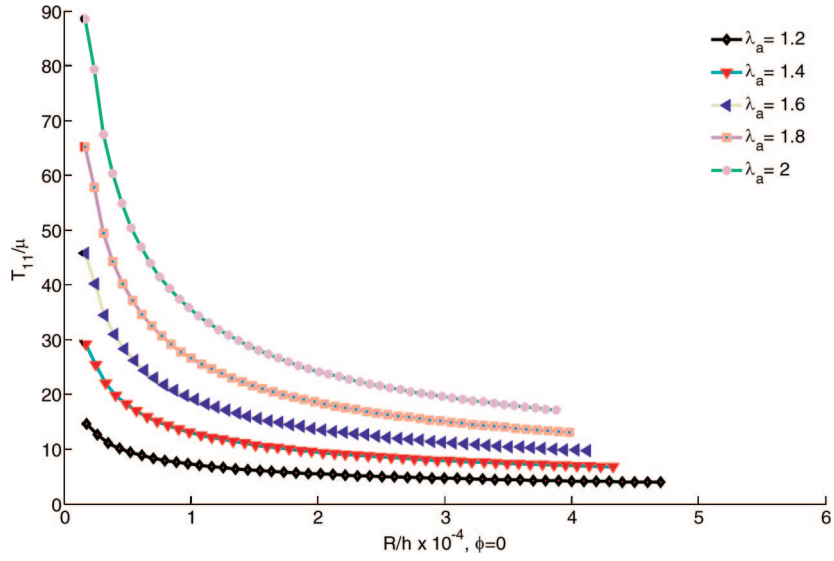

Figure 9. T_{11}/μ versus distance directly ahead of crack tip for $I_m = 3.5$.

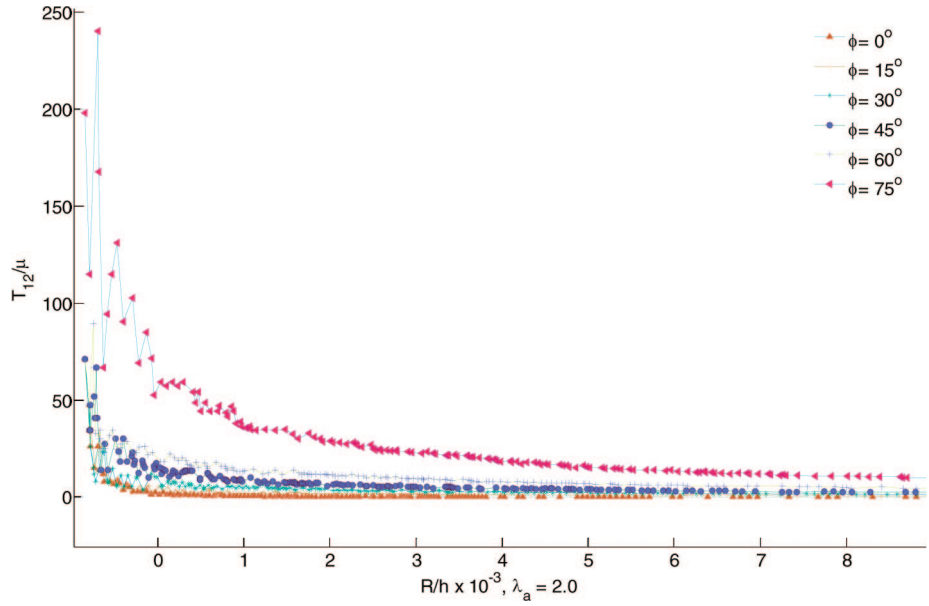

Figure 10. Plots of T_{12}/μ versus R/h for $I_m = 3.5$ along different radial paths specified by ϕ. The shear stress increases slightly with increasing angle for the same distance from the crack tip.

straight lines. These results are shown in Figure 8. A comparison of Figures 3b and 8 shows that $C(I_m,\lambda_a)$ is of order 1 and decreases to a constant value for large λ_a. Despite the large differences in strain hardening behavior, the near tip stress fields are very similar to the neo-Hookean solid. For example, $T_{22} \gg T_{11}$ (see Figures 7 and 9). Also, the shear stress T_{12} is vanishingly small in comparison with the normal stress T_{22} in the sector $|\phi| < \pi/2$ (see Figure 10). There is a slight difference between the two material models in that the shear stress on the deformed crack face $|\phi| = \pi/2$ is found to be very small, which is not the case for the neo-Hookean solid. As a consequence, elements *everywhere* suffer very little shear distortion, and this fact allows us to obtain accurate results even at large applied λ_a.

4. Summary and Discussion

The stress field near the tip of a plane stress crack in a strip fracture specimen loaded in mode I is studied for a neo-Hookean solid and an elastomer that strain hardens exponentially. Our calculations show that the near tip stress fields behave in a similar way despite the very large difference in strain hardening behaviors of the two material models. For example, the opening true stress (T_{22}) is much greater than the other normal stress component, T_{11}. In addition, the shear stresses are very small away from the crack face for both materials. However, there is a concentration of shear stress on the crack faces for the neo-Hookean solid which is not present in the exponentially hardening material. This suggests that shear deformation decreases with increasing strain hardening. In both materials, a uniaxial state of stress exists near the crack tip. Our simulation confirms that the crack tip stress field in soft materials is very different from the prediction of the linear theory.

Our numerical results for the exponentially hardening solid show that T_{22} directly ahead of the crack tip has a $-1/(R \ln R)$ singularity. Given that $\ln R$ is a very weak singularity, the opening stress singularities for the neo-Hookean and the exponential model are very similar. Also, in both material models, C_1 (C) approaches 1 for large applied stretches. Therefore, the amplitude of the dominant singular stress T_{22} is directly proportional to the energy release rate in this limit. The fact that they are so similar given the very different strain hardening behaviors suggests that this

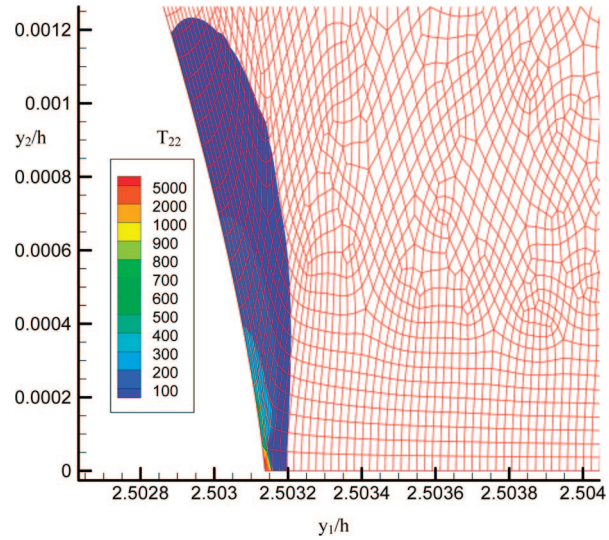

Figure 11. Normal opening stress (T_{22}) contour with FEM mesh is shown near the crack tip for $\lambda_a = 1.1$ in exponentially hardening solid ($I_m = 3.5$). The region where T_{22} is high is along the crack face rather than directly ahead of the crack tip, which suggests that secondary cracks may initiate from the crack face.

is a universal feature that is *approximately* satisfied for a wider class of soft materials, particularly for materials which exhibit high strain hardening. Exceptions will undoubtedly exist, and further investigation of this hypothesis is necessary. Figure 11 shows that there is a much bigger region along the crack face where the opening stress (T_{22}) is high than directly ahead of the crack tip for the exponential solid. Recall, for the neo-Hookean solid, (14a) shows that the opening stress has a higher singularity when approached along the crack face. This suggests that secondary cracks may initiate along the crack face. That is, it is possible for multiple crack fronts to develop ahead of the main crack. Crack tip splitting was indeed observed in some of the experiments of Seitz et al.[10]

The fact that the dominant crack tip stress field for both material models is similar does not imply that the deformation fields are

also similar. In fact, the exponential hardening material deforms much less. This can be quantified using the fact that T_{22} is

$$T_{22} = \mu W'(I)((y_{2,1} - \lambda^3 y_{1,2})y_{2,1} + (y_{2,2} - \lambda^3 y_{1,1})y_{2,2}) \tag{30a}$$

where $W' = \mathrm{d}W/\mathrm{d}I$. As one approaches the crack tip along $\phi = 0$

$$T_{22} \approx \mu(y_{2,2})^2 \exp[(y_{2,2})^2/I_m] \tag{30b}$$

for the exponential hardening model. Equations (30b) and (28) imply that

$$y_{2,2} \approx \sqrt{I_m \ln(T_{22}/\mu)} \propto \sqrt{-\ln R} \tag{30c}$$

Equation 30c implies that the deformation gradient for the exponential hardening model has a very weak logarithmic singularity. Using (30a), it can be shown that the deformation gradient for the neo-Hookean solid is $1/\sqrt{R}$. This means that the exponential hardening solid deforms much less as expected.

We include here a few remarks on criterion for crack propagation. A standard hypothesis is to assume that the applied energy release rate J is equal to the effective surface energy or fracture toughness of the material J_c. For the exponential hardening model, the crack growth criterion $J = J_c$ leads to

$$\lambda_a^* = \frac{\Gamma}{2} + \frac{\Gamma}{2}\sqrt{1 + \frac{1}{\Gamma^2}}, \qquad \Gamma = \sqrt{I_m \ln\left(1 + \frac{J_c}{\mu I_m h}\right)} \tag{31a}$$

where λ_a^* is the critical stretch for crack growth.

For large Γ

$$\lambda_a^* \approx \Gamma \approx \sqrt{I_m \ln\left(\frac{J_c}{\mu I_m h}\right)} \tag{31b}$$

Equations 23 and 27 and the fact that C_1 (C) approaches a constant for large λ_a suggest that this energy based fracture criterion is equivalent to a local stress based fracture criterion.

Acknowledgment. Support from Department of Energy Grant DE-FG02-07ER46463 is acknowledged by C.Y.H. This research was conducted using the resources of the Cornell University Center for Advanced Computing, which receives funding from Cornell University, New York State, the National Science Foundation, and other leading public agencies, foundations, and corporations. The authors would like to thank Ken Shull for discussions.

LA802795E